Dynamic transitions from smooth to rough to twinning in dislocation motion

JAIME MARIAN*[1,2], WEI CAI[1] AND VASILY V. BULATOV[1]

[1]Chemistry and Materials Science Directorate, Lawrence Livermore National Laboratory, 7000 East Avenue, Livermore, California 94551, USA
[2]Graduate Aeronautical Laboratories, California Institute of Technology, 1200 E. California Boulevard, Pasadena, California 91125, USA
*e-mail: jmarian@caltech.edu

Published online: 8 February 2004; doi:10.1038/nmat1072

The motion of dislocations in response to stress dictates the mechanical behaviour of materials. However, it is not yet possible to directly observe dislocation motion experimentally at the atomic level. Here, we present the first observations of the long-hypothesized kink-pair mechanism in action using atomistic simulations of dislocation motion in iron. In a striking deviation from the classical picture, dislocation motion at high strain rates becomes rough, resulting in spontaneous self-pinning and production of large quantities of debris. Then, at still higher strain rates, the dislocation stops abruptly and emits a twin plate that immediately takes over as the dominant mode of plastic deformation. These observations challenge the applicability of the Peierls threshold concept to the three-dimensional motion of screw dislocations at high strain rates, and suggest a new interpretation of plastic strength and microstructure of shocked metals.

Dislocations are ubiquitous line defects responsible for many properties of crystalline materials[1]. In response to an external load, dislocations move through the crystal producing a permanent change of shape (yield or plastic deformation). Generally, materials that yield can avoid a greater danger—catastrophic failure by fracture[2]. Consequently, exactly how dislocations move in response to stress has been a matter of serious concern and intensive study[3–10]. In a wider context, the dynamics of driven extended objects, that is, lines and interfaces, has also attracted much attention. From propagation of fire fronts[11], to surface growth[12], to motion of magnetic flux lines in superconductors[13,14], various phenomena were observed to display a similar dynamic behaviour often referred to as kinetic roughening[14,15]. The results that follow suggest that the motion of screw dislocations in iron displays a roughening transition that is a function of stress, temperature and dislocation line length.

By the very nature of slip, dislocation motion is confined to a glide plane defined by its slip (Burgers) vector $\mathbf{b}$ and its tangent vector $\boldsymbol{\xi}$ (Fig. 1). When $\boldsymbol{\xi}$ is locally parallel to $\mathbf{b}$ (screw orientation), the glide plane is not defined and the dislocation can in principle glide on any plane containing its Burgers vector. This ability to move in three dimensions makes screw dislocations special and has much to do with the ability of the dislocations to multiply under stress[16].

Given that direct experimental observations of dislocation motion at the atomic scale are still impossible, molecular dynamics (MD) is our method of choice for exploring the mechanistic intricacies of screw dislocation motion. To date, MD simulations have focused mostly on face-centred cubic (f.c.c.) metals, where dislocation lines are known to extend into ribbons of stacking faults on planes of the {111} type. This extension constrains all dislocations, including the screws, to remain on {111} planes except for relatively rare 'cross-slip' events in which the screws change their extension from one {111} plane to another[17,18]. Yet, in other materials, such as body-centred cubic (b.c.c.) metals, screw dislocations can exercise their distinctive ability to move in three-dimensional (3D) space much more freely than in f.c.c. metals. Given iron's pre-eminence as the king of structural materials and a well-documented critical role of screw dislocations in its plasticity and strength, we focus on the motion of screw dislocations in b.c.c. iron.

Figure 2 describes the set-up and results of our MD simulations in which we observed that depending on the magnitude of stress and

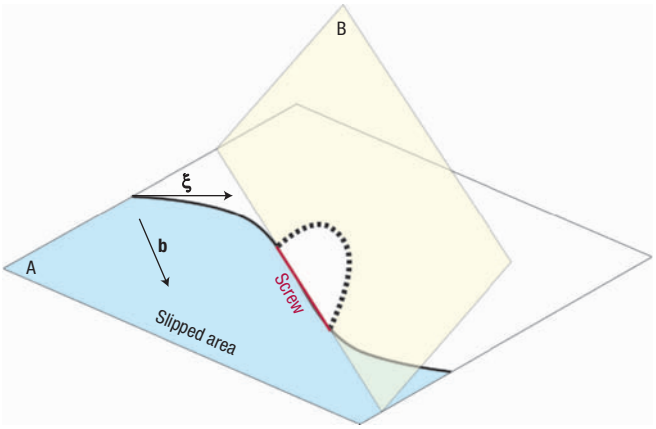

Figure 1 A dislocation made of disorder. To picture a dislocation, imagine a crystal sheared along plane A so that atoms just above the plane are displaced by an amount **b** relative to the atoms just below the plane. If **b** is a repeat vector of the crystal lattice, such slip re-establishes the perfect stacking of atoms everywhere except at the boundary between the slipped area and the rest of the plane. This boundary is a dislocation carrying a slip (Burgers) vector **b**. Dislocation segments with line direction **ξ** parallel to **b** are called screws. Screws can principally move into any plane (such as B) that contains **b**.

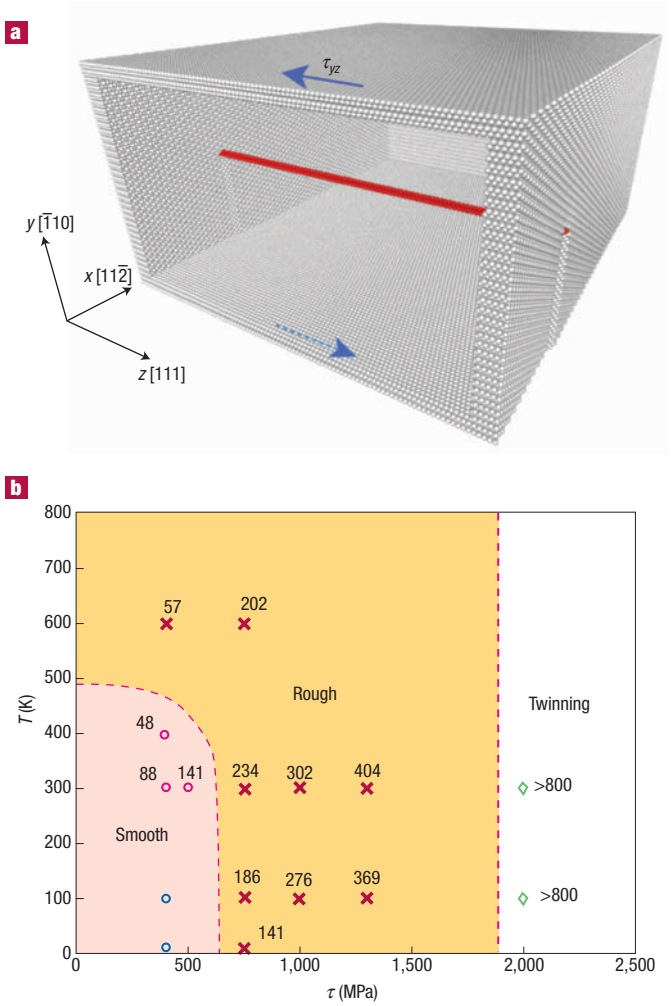

Figure 2 Simulation setup and results. a, View of the simulation box used in the calculations. Dislocation core atoms (red) differ from all other atoms by their relatively large centro-symmetry-deviation parameter[41]. To show the dimensions of the model crystal, several layers of atoms at the box boundaries are also plotted (grey). The solid and dashed blue arrows indicate the direction of the applied stress. **b**, Average screw dislocation velocities (in m s^{-1}) in our MD simulations at different temperature and stress conditions. Different symbols are used to indicate different dislocation behaviour observed: pink circles for smooth motion (Fig. 3), red crosses for rough motion (Fig. 4), and green diamonds for twinning (Fig. 6). Blue circles correspond to cases where no dislocation motion was observed during the entire course of the simulation. The dashed lines delineate estimated conditions for transitions from one type of behaviour to another. Estimated strain rates for these simulations are 30 to 10^8 s^{-1}.

temperature, screw dislocations in b.c.c. iron move in three strikingly different regimes. First, under low stress, the dislocations move smoothly through the formation and migration of atomic-sized kinks (Fig. 3). Although widely accepted, this is to our knowledge the first time that such mechanism of motion has been directly observed in full dynamic detail. As the stress is further increased, dislocation motion suddenly becomes rough: the line becomes rugged and its motion becomes jerky, producing in its wake a large amount of debris in the form of lattice vacancies and interstitial clusters (Figs 4,5). Under still higher stress, the line ruggedness and the amount of debris its motion produces continue to increase until, at some point, another dynamic transition takes place. The dislocation is now seen to cease its 'turbulent' motion, and to initiate a thin plate of sheared crystal, a twin (Fig. 6). The twin starts where the dislocation just left off, extending rapidly along the same direction as that of the dislocation motion, and gradually increases in thickness. In what follows, the atomistic origins of these dynamical transitions and their dependence on applied stress, temperature and dislocation length are discussed. All the figures are discussed in detail below.

Let us first consider the regime in which the screw moves in a smooth, 'laminar' manner. As a useful point of reference, the lattice resistance to dislocation motion is commonly characterized in terms of its Peierls threshold τ_P, that is, a minimal stress required to make the dislocation move at 0 K (refs 1,19). For the screw dislocation in our model of b.c.c. iron, τ_P = 900 MPa (ref. 20) (see Methods). However, the dislocation is able to move under lower stress, provided its motion is aided by thermal fluctuations. Figure 3 contains a series of snapshots of the screw motion at room temperature (300 K) under a stress τ = 500 MPa, significantly below the Peierls threshold. In Fig. 3b, a portion of the line jumps to the next lattice position (Peierls valley) forming a pair of atomic-sized kinks. Driven by stress, the kinks then rapidly migrate along the dislocation line (Fig. 3c) and eventually recombine through the periodic boundary. As a result, the entire dislocation translates to the next lattice position (Fig. 3d). To our knowledge, this entire sequence is the first unambiguous demonstration of the long-hypothesized kink-pair mechanism in action[1,21].

At higher stress and/or temperature, the character of dislocation motion changes dramatically (Fig. 4). The line becomes corrugated and grows increasingly uneven, developing multiple pinning points in its path. Dynamically, the dislocation now moves in bursts, breaking away from one pinning point to another, each time covering several lattice distances and leaving behind pieces of debris. The debris consists of vacancy and self-interstitial clusters ranging in size from single vacancies and interstitials (at low temperatures) to large vacancy and interstitial clusters (at higher temperatures). What causes this sudden change of behaviour? A meticulous analysis of the simulation snapshots revealed the underlying mechanism. This is described below using a representative sequence of events observed in a separate

zero-temperature simulation in which the initial pinning was introduced 'by hand'. By disposing of the thermal noise, the succession of events leading to roughening and debris formation stands out clear and unmasked (Fig. 5).

Self-pinning and the subsequent roughening are triggered by collisions of kinks gliding towards each other on two different planes. In Fig. 5a, the sequence begins when two kink pairs, 1–2 and 3–4, form, not necessarily simultaneously, at two different positions along the line. Unlike the screw dislocation itself, the kink segments are not parallel to the Burgers vector **b**. Therefore, once nucleated on a plane, a kink pair remains constrained to glide on that very same plane. If two kink pairs happen to nucleate on the same plane, opposing kinks will move towards each other and recombine when they collide (in the same way as in Fig. 3c). However, if two kink pairs nucleate on two different planes, colliding kinks find each other on two different glide planes, unable to recombine, resulting in a peculiar 'conflict' configuration with the two kinks pushing and blocking each other, such as kinks 2 and 3 in Fig. 5b. After the work of Louchet *et al.*[22], we shall call such conflict configurations 'cross-kinks' (CK).

In b.c.c. crystals, kink pairs can nucleate on three distinct {110} planes parallel to the $\frac{1}{2}\langle 111\rangle$ Burgers vector[1,21,23]. Taking into account this threefold rotational symmetry of the b.c.c. lattice, in this quasi-static simulation we selected a shear-stress direction in such a way that kink-pair nucleation becomes equally likely on two of the three planes, whereas on the third plane kink nucleation is prevented. In such conditions, the likelihood of CK formation increases due to more frequent collisions of kinks nucleated on two competing planes. Furthermore, as two colliding kinks (2 and 3 or 1 and 4 in Fig. 5b) feel equal forces pushing them against each other, the CKs remain stationary and act as strong pinning points dividing the line into two segments stretching along two different lattice valleys (P_2 and P_3 in Fig. 5). To continue its motion, the dislocation has to somehow disentangle itself from the CK. Presumably, if the two line segments are bent (kinked) further onto the same valley, say P_4, the line could reconnect and the conflict would be resolved. For this to happen, each of the two segments should generate at least two more kink pairs on suitable planes. Shown in Fig. 5c is one such kink pair 7–8 that brings one of the two segments from valley P_2 to valley P_4. Likewise, kink pair 5–6 brings the other segment from P_3 to P_4.

It turns out that, although the two leading segments of the screw dislocation have moved to the same valley P_4 (Fig. 5c), they remain disconnected even under stresses up to the Peierls threshold of 900 MPa. Below the Peierls stress, reconnection takes place only when more kinks pile up on both sides of the conflict. For example in Fig. 5d, two extra kink pairs bring the leading segment to valley P_5. After that, it takes only 400 MPa to force the reconnection of two screw segments around one of the two CKs (Fig. 5e). After reconnection, the CK transforms into a closed loop of atomic dimensions detached from the main dislocation line. This piece of debris is the price the dislocation pays for disentangling itself from the CK.

In the case shown in Fig. 5e, the debris loop is nothing but a single lattice vacancy. However, given the stochastic nature of kink-pair nucleation, the CK conflicts can be resolved through the formation of larger debris loops. The resulting closed loops are prismatic, that is, with Burgers vector perpendicular to the loop plane, and come in two varieties, vacancy (V)-loops and self-interstitial (SI)-loops, depending on the loop directionality. A V-loop is a plate of empty lattice sites grouped together, whereas an SI-loop is a plate of extra atoms inserted into the lattice. We note that the other CK shown in Fig. 5e should, on closure, produce a single interstitial. However, it remains open for stresses up to the Peierls threshold. The relative difficulty in closing SI-loops compared with V-loops derives from the higher interstitial formation energy (5.0 eV) compared with that of a vacancy (1.7 eV) (ref. 24). This is consistent with our MD simulations that reveal a clear asymmetry: whereas V-conflicts are readily resolved through the formation of small V-loops, self-pinning by SI-conflicts is obviously much stronger. As a result, SI-loops are typically much larger than V-loops, such as in Fig. 4. We note in passing that the details of the self-pinning and break-away mechanisms can be affected if the core of screw dislocations experiences a symmetry-breaking reconstruction, also known as core polarization[21]. However, we leave the possible implications of core polarization for the dislocation roughening behaviour open for further research.

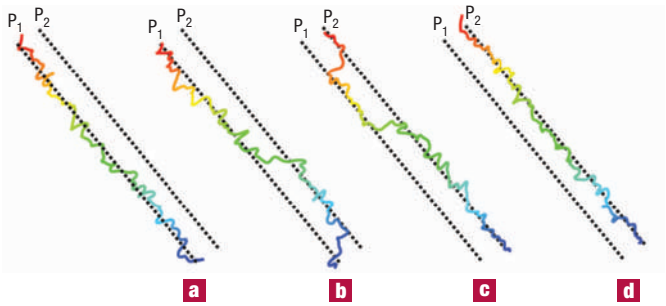

Figure 3 The kink-pair mechanism of smooth dislocation motion at 300 K and τ_{yz} = 500 MPa. The line connects the centres of mass of dislocation core atoms (red in Fig. 2a) computed for every atomic-sized slice of the crystal along the *z* direction. The dislocation is colour-graded according to its distance from the bottom end, and shrunk by a factor of 10 for better visualization. **a**, At 20.9 ps, the dislocation line lies mostly along the initial Peierls valley P_1. The wiggles on the line profile are due to thermal noise and are visibly smaller than the distance to the next Peierls valley P_2. **b**, At 21.5 ps, a kink-pair nucleates (in the blue region). **c**, At 22.5 ps, the kinks have swept through most of the line. One of the kinks (blue in part **b**) has now moved across the periodic boundary (now in red). **d**, At 23.5 ps, the two kinks recombine after which the entire dislocation lies in the next Peierls valley P_2.

Remarkably, the observed mechanisms of V- and SI-loop formation do not involve any vacancy or interstitial diffusion, either into or out of the moving dislocation. Instead, the defects form by shifting rows of atoms relative to each other along the line direction. Once the loop is closed, the dislocation can continue to move ahead by detaching itself from the loop that is now left behind. Because the average line direction in our simulations is exactly along the Burgers vector, the total numbers of vacancies and interstitials contained in the debris loops must be and are exactly equal.

Having identified the atomistic mechanisms of self-pinning and debris loop formation, let us try to predict the conditions for the roughening transition. For this, it is useful to compare the dislocation line length L to the kink mean-free path λ. The latter is the statistically averaged distance a kink travels from its nucleation to a collision with another kink. For a self-pinning event to occur, there must be at least two or more kink pairs on the dislocation line simultaneously. Obviously no roughening is expected when $\lambda > L$. However, there will be a reasonable chance for two or more kink-pairs to co-exist and, at least occasionally, move on two different planes, if $\lambda \sim L$. According to the kink-diffusion model[1], $\lambda = \sqrt{(v_k/J_k)}$, where v_k is the kink migration velocity and J_k is the kink-pair nucleation rate. Below the Peierls stress, kink nucleation is thermally activated and, therefore, J_k should increase exponentially with increasing temperature and/or stress. At the same time, kink migration is limited by viscous drag[25], so that v_k should increase only linearly with stress, and even decrease with increasing temperature. Overall, λ must decrease sharply with increasing temperature and/or increasing stress. This is entirely consistent with our findings (Fig. 2b) that for a given dislocation length ($100b$, where b is the modulus of the Burgers vector), a transition from smooth to rough behaviour occurs both as the stress

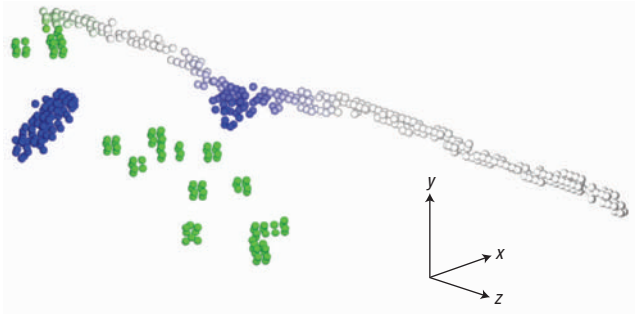

Figure 4 Rough motion and debris production. MD snapshot at 300 K, $\tau_{yz} = 750$ MPa. Dislocation core atoms are white, atoms surrounding the vacancies are green and atoms in and around the interstitial clusters are blue.

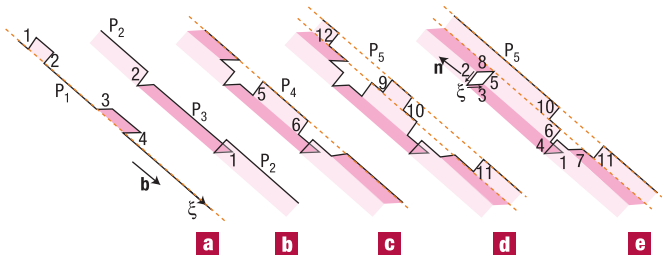

Figure 5 Cross-kink mechanism of self-pinning and debris production. A dynamic sequence in which cross-kink formation leads to self-pinning, roughening and debris production. The areas swept by dislocation kinks on two different planes are shaded using two different colours. ***n*** is the loop's plane normal.

increases from 400 MPa to 750 MPa at a fixed temperature (400 K and below), and as the temperature increases from 400 K to 600 K at a fixed stress (400 MPa). Furthermore, roughening can also be induced by directly varying the dislocation length L. For instance, at 300 K and $\tau = 750$ MPa, the motion of a dislocation of length $L = 100b$ is rough, whereas a shorter dislocation with $L = 50b$ moves smoothly under the same conditions. These findings confirm that the cross-kink mechanism is responsible for the smooth-to-rough transition and, in hindsight, emphasize how important it was to allow dislocations to move in 3D motion by considering sufficiently long lines. Needless to say, quasi-2D simulations of very short dislocations ($L < 10b$) commonly performed thus far[26] show no roughening transition under any conditions of stress and temperature.

There is ample experimental evidence for point-defect production by plastic deformation in both b.c.c.[27,28] and f.c.c. metals[29,30], although the origin of the debris remains unclear. The conventional thinking is that point defects are produced by some factors extrinsic to the moving dislocation, such as dragging pre-existing jogs[1,31] (steps out of the glide plane) or interactions with strong obstacles[32,33]. However, these can hardly explain the large quantities of defect clusters as well as their relatively uniform spatial distribution[27]. Contrary to this common perception, here we find that spontaneous roughening of perfectly straight dislocations produces many point defects and defect clusters (dislocation loops) in the absence of any other defects or obstacles. Unlike the roughening transition in the motion of magnetic flux lines in superconductors[14], we find that, at least in b.c.c. metals such as iron, roughening and the ensuing debris production are intrinsic behaviours of screw dislocations whose occurrence is regulated by temperature, stress and their own lengths.

The general trend of experimental data is consistent with our simulation results: for example, more debris is formed at higher deformation rates[34] (and hence higher stress), especially in shocked materials. Our results suggest that in b.c.c. metals, point-defect production signals the occurrence of rough dislocation motion. The intensity of debris production can be quantified by the fraction of mechanical work expended by the applied stress on defect formation. This fraction lies between 15% and 20% in our simulations, although some part of the debris is likely to disappear quickly by way of mutual recombination of vacancy and interstitials. The latter are seen to move even on the short (~100 ps) time scale of our MD simulations, and may consume a large part of the less mobile vacancies immediately after the dislocation passage, well before any observation can be made. Further evolution of defects produced by screw dislocation motion is likely to be similar to that in irradiated metals[35].

In the classical picture, the Peierls threshold stress τ_P marks a transition between distinctly different mechanisms of dislocation motion: thermally activated kink-pair mechanisms[1] below τ_P and the viscous phonon-drag mechanisms[36] above τ_P. Remarkably, in the range of conditions where dislocation motion is observed to be rough, dislocation velocity is proportional to stress, $v = \tau b/B$ (where B is the drag coefficient), similar to that in the phonon-drag behaviour. However, the effective resistance to dislocation motion is now defined by dislocation self-pinning and unpinning, leading to an effective drag coefficient about 2.5 times higher than when the resistance is indeed limited by the phonon-drag alone (see Methods). The behaviour remains essentially the same both below and above τ_P: the dominance of the rough motion mechanisms makes the classical transition at Peierls threshold essentially disappear. This observation calls into question the significance of the Peierls stress concept for characterization of the motion of screw dislocations in b.c.c. metals.

We now come to the second dynamic transition observed under a still higher stress of 2.0 GPa. Figure 6a shows a snapshot of this simulation in which the initial screw dislocation is at the trailing edge of a thin twinning plate (on the left). The leading edge of the twin is propagating to the right, and consists of three twinning $\frac{1}{6}\langle 111\rangle$ partial dislocations staggered on top of each other on three adjacent {112} planes, as in Fig. 6b. This observation is entirely consistent with an earlier proposed mechanism[37,38]. For a few moments preceding twin nucleation, the screw moves over several lattice valleys producing a few pieces of debris. However, after the twinning plate forms, the debris production ceases at once whereas the velocity of twin propagation jumps to ~800 m s^{-1}, compared with 400 m s^{-1} for the rough dislocation motion observed below 2.0 GPa. With time, the twinning plate grows thicker through the formation of twinning dislocation dipoles on the plate surfaces. Comparing the stress at which twinning is initiated here (2.0 GPa) with the stress at which the same material twins in the absence of pre-existing dislocations (5.6 GPa), we conclude that screws can be very effective sources of twinning nucleation. Short dislocations, for example, $L = 5b$, do not produce twinning but continue to move smoothly, although with very high velocities, under the same temperature and stress conditions. It appears that roughening of long dislocations observed just before the twinning commences is not accidental. Evidently, roughening slows the screw down to such an extent that it is no longer able to relieve the strain by its motion alone. At the same time, the same screw serves as a preferable site for twinning nucleation, which immediately takes over as the leading mechanism of plastic response.

In a series of large-scale MD simulations, long screw dislocations in b.c.c. iron move in ways that are dramatically different from the idealized motion of very short, straight dislocations nearly exclusively considered thus far. Depending on stress and temperature, dislocation motion proceeds through unusual previously unknown mechanisms

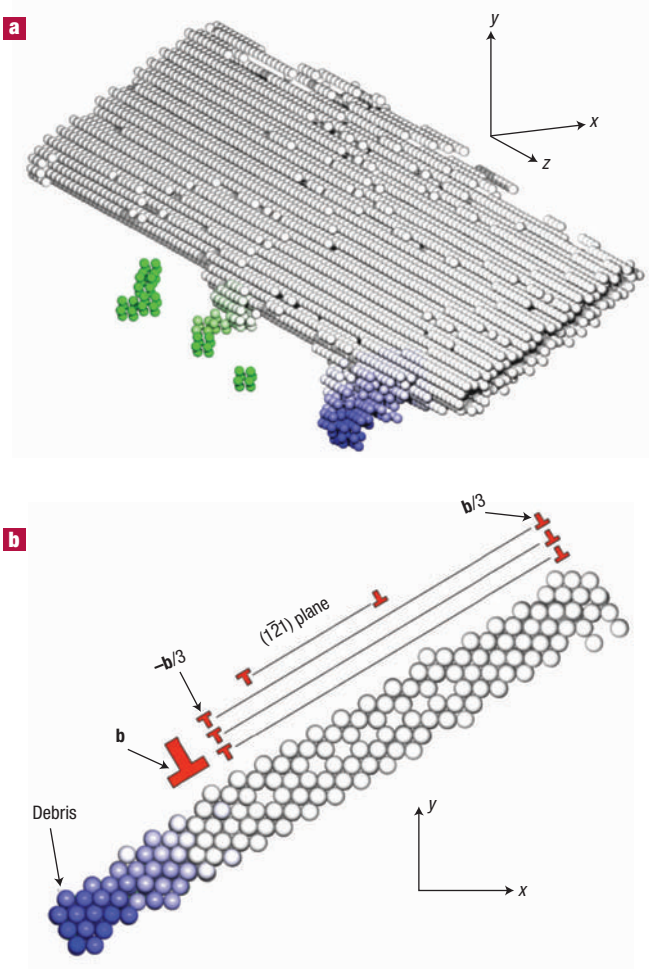

Figure 6 Twinning initiation by dislocation. Snapshots of the MD simulation at 300 K, $\tau_{yz} = 2{,}000$ MPa, and 20 ps showing twinning initiation. **a**, Image of the twinning plate with debris left near where the dislocation starts its motion. **b**, View along the direction of the Burgers vector. The three twinning $\frac{1}{6}\langle 111\rangle$ partial dislocations sitting on consecutive {112} planes are shown schematically.

involving dislocation self-pinning, roughening and debris loop formation. These mechanisms are notably diffusionless and intrinsic to the screw dislocations themselves. The resulting dislocation mobility does not exhibit a commonly anticipated transition to phonon-drag mechanisms above the Peierls threshold stress. Instead, the mobility is limited by self-pinning and debris formation, both below and above the Peierls stress. Under still higher stress, twinning initiation and propagation supplants screw dislocation motion as the dominant plasticity carrier. These behaviours are expected to define the plastic resistance of b.c.c. metals in high-rate deformation conditions, such as under shocks.

METHODS

MOLECULAR DYNAMICS SIMULATION PROCEDURE

MD simulations were performed in a b.c.c. crystal with ~800,000+ Fe atoms interacting with each other through the Ackland-Finnis-Sinclair potential[24]. The crystal's dimensions are $x = 40 \times [11\bar{2}]$, $y = 34 \times [\bar{1}10]$, $z = 100 \times \frac{1}{2}[111]$. A screw dislocation with $\mathbf{b} = \frac{1}{2}[111]$ is introduced along z. The crystal is periodic along x and z and has free surfaces as upper and lower bounds in the y direction. To entice the dislocation to move, shear stress τ_{yz} is applied through forces on several atomic layers at the free surfaces. Simulations are carried out by integrating Newton's equations of motion[39] for all atoms using a time step of 1 fs. A typical simulation continues for about 100 ps over which the temperature is kept constant through coupling to a thermostat[40].

CALCULATION OF THE PEIERLS STRESS

We performed a series of quasi-static, energy-minimization calculations on a dislocation structure under different stress magnitudes using the Parrinello–Rahman scheme[40]. The Peierls stress, τ_p, was taken as the lowest stress at which dislocation motion occurs[20].

ESTIMATION OF THE STRAIN RATE

The dislocation density directly derived from our simulations is unrealistically high due to the severe size limitations of MD. However, proper treatment of the boundary conditions assures that for as long as the dislocation moves under stresses and temperatures similar to those encountered in real crystals, the behaviours observed in simulations like ours should be representative of much lower dislocation densities and, hence, much lower strain rates. Therefore, to make a connection with experiments, our simulations must be placed in the proper context and the range of strain rates to which they correspond must be estimated. Orowan's equation states that the plastic strain rate $d\tilde{\varepsilon}/dt$ is the product of the mobile dislocation density ρ_m times the dislocation velocity v and the Burgers vector $\mathbf{b}$ ($\sim 3 \times 10^{-10}$ m). Given that the dislocation moves at about 10 to 400 m s^{-1} in our simulations, and that experimentally measured dislocation densities typically range from 10^{10} to 10^{15} m^{-1}, our simulations should correspond to experiments performed at strain rates ranging from 30 to 10^8 s^{-1}.

CALCULATION OF THE PHONON-DRAG COEFFICIENT

The phonon-drag coefficient, B_{ph}, was calculated from the slope of the stress–velocity data obtained for several values of stress above τ_p. In these calculations we used short ($<10b$) dislocation segments to suppress kink-pair formation and roughening. The resulting phonon-drag coefficient is 3.0×10^{-4} Pa s, considerably smaller than the value of $\sim 7.5 \times 10^{-4}$ Pa s obtained for the resistance coefficient in the rough motion regime of long ($100b$) lines.

Received 1 October 2003; accepted 17 December 2004; published 8 February 2004.

References

1. Hirth, J. P. & Lothe, J. *Theory of dislocations* (Wiley, New York, 1982).
2. Kuhlmann-Wilsdorf, D. & Wilsdorf, H. G. F. Dislocation movements in metals. *Science* **144,** 17–25 (1964).
3. Bullough, R. & Tewary, V. K. in *Dislocations in Solids* Vol. 2 (ed. Nabarro, F. R. N.) Ch. 5 (North-Holland, Amsterdam, 1979).
4. Duesbery, M. S. in *Dislocations in Solids* Vol. 8 (ed. Nabarro, F. R. N.) Ch. 39 (North Holland, Amsterdam, 1989).
5. Bulatov, V. V., Abraham, F. F., Kubin, L., Devincre, B. & Yip, S. Connecting atomistic and mesoscale simulations of crystal plasticity. *Nature* **391,** 669–672 (1998).
6. Zhou, S. J., Preston, D. L., Lomdahl, P. S. & Beazley, D. M. Large-scale molecular dynamics simulations of dislocation intersection in copper. *Science* **279,** 1525–1527 (1998).
7. Gumbsch, P. & Gao, H. Dislocations faster than the speed of sound. *Science* **283,** 965–968 (1999).
8. Diaz de la Rubia, T. *et al.* Multiscale modelling of plastic flow localization in irradiated metals. *Nature* **406,** 871–874 (2000).
9. Miguel, M.–C., Vespignani, A., Zapperi, S., Weiss, J. & Grasso, J.–R. Intermittent dislocation flow in viscoplastic deformation. *Nature* **410,** 667–671 (2001).
10. Li, J., Van Vliet, K. J., Zhu, T. & Yip, S. Atomistic mechanisms governing elastic limit and incipient plasticity in crystals. *Nature* **418,** 307–310 (2002).
11. Maunuksela, J. *et al.* Kinetic roughening in slow combustion of paper. *Phys. Rev. Lett.* **79,** 1515–1518 (1997).
12. Barabasi, A.-L. & Stanley, H. E. *Fractal Concepts in Surface Growth* (Cambridge Univ. Press, Cambridge, UK, 1995).
13. Tonomura, A. *et al.* Motion of vortices in superconductors. *Nature* **397,** 308–309 (1999).
14. Surdeanu, R. *et al.* Kinetic roughening of penetrating flux fronts in high-T_c thin film superconductors. *Phys. Rev. Lett.* **83,** 2054–2057 (1999).
15. Kardar, M., Parisi, G. & Zhang, Y.–C. Dynamic scaling of growing interfaces. *Phys. Rev. Lett.* **56,** 889–892 (1986).
16. Devincre, B. & Kubin, L. P. Mesoscopic simulations of dislocations and plasticity. *Mater. Sci. Eng. A* **234,** 8–14 (1997).
17. Duesbery, M. S. Dislocation motion, constriction and cross-slip in fcc metals. *Model. Simul. Mater. Sci.* **6,** 35–49 (1998).
18. Vegge, T., Rasmussen, T., Leffers, T., Pedersen, O. B. & Jacobsen, K. W. Atomistic simulations of cross-slip of jogged screw dislocations in copper. *Phil. Mag. Lett.* **81,** 137–144 (2001).
19. Peierls, R. E. The size of a dislocation. *Proc. Phys. Soc.* **52,** 34–37 (1940).
20. Marian, J. *Improved Understanding of Radiation Damage in Ferritic Alloys: A Multiscale Modeling Study* Thesis, Universidad Politécnica de Madrid (2002).
21. Ngan, A. H. W. & Wen, M. Dislocation kink-pair energetics and pencil glide in body-centered-cubic crystals. *Phys. Rev. Lett.* **87,** 075505 (2001).
22. Louchet, F. & Viguier, B. Ordinary dislocations in γ-TiAl: cusp unzipping, jog dragging and stress anomaly. *Phil. Mag. A* **80,** 765–779 (2000).
23. Vitek, V. Theory of core structures of dislocations in body-centered cubic metals *Cryst. Latt. Def. Amorp.* **5,** 1–34 (1974).
24. Ackland, G. J., Bacon, D. J., Calder, A. F. & Harry, T. Computer simulation of point defect properties in dilute Fe-Cu alloy using a many-body interatomic potential. *Phil. Mag. A* **75,** 713–732 (1997).
25. Chang, J., Cai, W., Bulatov, V. V. & Yip, S. Molecular dynamics simulations of motion of edge and screw dislocations in a metal. *Comp. Mater. Sci.* **23,** 111–115 (2002).
26. Woodward, C. & Rao, S. I. Flexible *ab initio* boundary conditions: simulating isolated dislocations in bcc Mo and Ta. *Phys. Rev. Lett.* **88,** 216402 (2002).
27. Kaufmann, H.-J., Luft, A. & Schulze, D. Deformation mechanism and dislocation structure of high-purity molybdenum single-crystals at low temperatures. *Cryst. Res. Technol.* **19,** 357–372 (1984).
28. Pal-Val P. P. & Kauffman, H.-J. Variation of low-temperature internal-friction at microplastic deformation of high-purity molybdenum single-crystals. *Cryst. Res. Technol.* **19,** 1049–1055 (1984).
29. Dai, Y. & Victoria, M. Defect structures in deformed FCC metals. *Acta Mater.* **45,** 3495–3501 (1997).

30. Kiritani, M. *et al.* Anomalous production of vacancy clusters and the possibility of plastic deformation of crystalline metals without dislocations. *Phil. Mag. Lett.* **79,** 797–804 (1999).
31. Vegge, T., Leffers, T., Pedersen, O. B. & Jacobsen, K. W. Atomistic simulations of jog migration on extended screw dislocations. *Mater. Sci. Eng. A* **319,** 119–123 (2001).
32. Hirsch, P. B. & Humphrey, F. J. Deformation of single crystals of copper and copper-zinc alloys containing alumina particles. 1. Macroscopic properties and work hardening theory. *Proc. R. Soc Lon. A* **318,** 45–72 (1970).
33. Bacon, D. J., Kocks, U. F. & Scattergood, R. O. Effect of dislocation self-interaction on Orowan stress. *Philos. Mag.* **28,** 1241–1263 (1973).
34. Hsiung, L. M. & Lassila, D. H. Initial dislocation structure and dynamic dislocation multiplication in Mo single crystals. *CMES-Comp. Model. Eng.* **3,** 185–191 (2002).
35. Odette, G. R. Wirth, B. D., Bacon, D. J. & Ghoniem, N. M. Multiscale-multiphysics modeling of radiation-damaged materials: embrittlement of pressure-vessel steels. *Mater. Res. Soc. Bull.* **26,** 176–182 (2001).
36. Alshits, V. I. & Indenbom, V. L. in *Dislocations in Solids* Vol. 7 (ed. Nabarro, F. R. N.) Ch. 34 (North-Holland, Amsterdam, 1986).
37. Sleeswyk, A. F. 1/2[111] screw dislocations and nucleation of [112][111] twins in the bcc lattice. *Philos. Mag.* **8,** 1467–1486 (1963).
38. Lagerlof, K. P. D. On deformation twinning in bcc metals. *Acta Metall. Mater.* **41,** 2143–2151 (1993).
39. Allen, M. P. & Tildesley, D. J. *Computer Simulation of Liquids* (Clarendon, Oxford, UK, 1989).
40. Hoover, W. G. Canonical dynamics: equilibrium phase-space distributions. *Phys. Rev. A* **31,** 1695–1697 (1985).
41. Kelchner, C. L., Plimpton, S. J. & Hamilton, J. C. Dislocation nucleation and defect structure during surface indentation. *Phys. Rev. B* **58,** 11085 (1998).

Acknowledgements

This work was performed under the auspices of the US Department of Energy by Lawrence Livermore National Laboratory under Contract W-7405-Eng-48.
Correspondence and requests for materials should be addressed to J.M.

Competing financial interests

The authors declare that they have no competing financial interests.